[Short title + Author Name - P&H title] 32 (2024) 101940

HOSTED BY

Contents lists available at ScienceDirect

Saudi Pharmaceutical Journal

journal homepage: www.sciencedirect.com

α-glucosidase and α-amylase inhibitory activity of flavonols from *Stenochlaena palustris* (Burm.f.) Bedd

Rudi Hendra [a,b,*], Monika Kerry Army [a,c], Neni Frimayanti [d], Hilwan Yuda Teruna [a], Rizky Abdulah [b,e], Ari Satia Nugraha [f]

[a] Department of Chemistry, Faculty of Mathematics and Natural Sciences, Universitas Riau, Pekanbaru, Indonesia
[b] Center of Excellence in Pharmaceutical Care Innovation, Universitas Padjadjaran, Bandung, Indonesia
[c] National Agency of Drug and Food Control, Jakarta, Indonesia
[d] Sekolah Tinggi Ilmu Farmasi Riau, Pekanbaru, Indonesia
[e] Department of Pharmacology and Clinical Pharmacy, Faculty of Pharmacy, Universitas Padjadjaran, Jatinangor, Indonesia
[f] Drug Utilisation and Discovery Research Group, Faculty of Pharmacy, University of Jember, Jember, Indonesia

ARTICLE INFO

Keywords:
Flavonols
Stenochlaena palustris
α-glucosidase and α-amylase inhibition
In silico

ABSTRACT

Stenochlaena palustris (Burm.f.) Bedd., a fern species native to India, Southeast Asia, Polynesia, and Australia, has a long history of medical including as a diabetic therapy. This study aimed to isolate bioactive compounds from *S. palustris* ethyl acetate extract and assess their *in vitro* and *in silico* inhibitory activities against α-glucosidase and α-amylase. The successful separation of five flavonols, namely stenopalustroside A (**1**), tiliroside (**2**), kaempferol (**3**), quercetin (**4**), and rutin (**5**), was achieved through phytochemical analysis. The compounds exhibited a range of inhibitory activities against α-glucosidase and α-amylase, with IC_{50} values ranging from 40 to 250 μg/mL. Notably, the biological activities of compound **1** have been reported for the first time. Compound **4** was the most effective inhibitor of both enzymes among the isolated compounds. Studies performed *in silico* reveal that the interactions between amino acids in compounds **4** and **5** are remarkably comparable to those observed in the positive control. These compounds share this commonality, and as a result, they both have the potential to be active agents.

1. Introduction

Diabetes mellitus (DM) is a metabolic disorder characterized by chronic hyperglycaemia and carbohydrate, fat, and protein metabolism disruptions. Flaws in either insulin secretion or insulin action cause these metabolic disorders. In 2021, there were 537 million people with a confirmed diagnosis of diabetes, and early projections indicate that there will be 783 million cases by 2045 (Dysted et al., 2021). This occurrence is the result of population dietary and lifestyle changes. Diabetes mellitus (DM) causes severe cardiovascular complications as well as diabetic nephropathy, diabetic retinopathy, and neuropathy. Long-term complications of diabetes mellitus (DM) include organ damage, organ dysfunction, and organ failure (World Health Organization, 1999, Tran et al., 2020, Sukhikh et al., 2023). When the human body develops insulin resistance and sugar accumulates in the blood, it is considered type 2 diabetes. In contrast, type 1 diabetes is characterized by the immune system's attack and destruction of pancreatic cells (Neeland and Patel, 2019).

Diet and lifestyle changes can control plasma glucose levels in type 2 diabetes by stimulating insulin secretion, slowing starch digestion, and interrupting or slowing blood sugar absorption from the small intestine (Kim et al., 2014). This can be accomplished by inhibiting the activities of enzymes involved in the digestion of dietary starch into glucose, such as α-amylase and α-glucosidase. These enzymes' activity is inhibited by enzyme inhibitors such as acarbose, miglitol, and voglibose. Alternative treatments are required to avoid side effects of these drugs, such as gastrointestinal distress (Rosak and Mertes, 2012).

There is evidence that demonstrates that plants, fruits, vegetables, and fungi are a significant source of secondary metabolites with known α-amylase and α-glucosidase inhibitory activities, including anthocyanins, coumarin, flavonoids, phenolic acids, saponins, carotenoids, terpenes, and alkaloids (Chen et al., 2018, Karakaya et al., 2018). For

Peer review under responsibility of King Saud University.
* Corresponding author.
E-mail address: rudi.hendra@lecturer.unri.ac.id (R. Hendra).

https://doi.org/10.1016/j.jsps.2023.101940
Received 17 September 2023; Accepted 25 December 2023
Available online 27 December 2023

example, the publication by El Ridhasya et. Al (2020) reported *Helminthostachys zeylanica*, a fern-like plant of the Ophioglossaceae, is used in traditional medicine in Southeast Asia and China to treat diabetes mellitus (DM), and it was found that prenylated flavonoids, Ugonin J and K exhibited α-glucosidase inhibitory activity. (Chang et al., 2019, El Ridhasya et al., 2020). Berberine is another example of an alkaloid that improves insulin resistance by inhibiting the hypothalamic–pituitary–adrenal pathway (Zhou et al., 2021).

Stenochlaena palustris (Burm.f.) Bedd. (Blechnaceae) or *paku kelakai* in Indonesia, a fern species with known medicinal and culinary applications indigenous to regions such as India, Southeast Asia, Polynesia, and Australia, has been traditionally employed as a therapeutic agent for diabetes mellitus (DM), treat fever, sore throat, and gastric ulcers. The existing literature provides substantial evidence for the antioxidant and anti-plasmodial properties in the phytochemical extracts of *S. palustris*. In particular, the dichloromethane and ethyl acetate fractions have exhibited noteworthy levels of anti-plasmodial activities and free radical scavenging capabilities (Hendra et al., 2022). Liu et al. have isolated ten acylated flavonol glycosides from the leaves of *S. palustris*, which demonstrated a spectrum of antibacterial activities, specifically against Gram-positive bacterial strains (Liu et al., 1999). Moreover, previous reports suggest that the ethyl acetate and aqueous fractions of this fern species show potent α-glucosidase inhibitory activities (Chai et al., 2015); however, a comprehensive identification of the secondary metabolites responsible for this bioactivity is yet to be conducted. As part of our ongoing research into natural products derived from Indonesian medicinal plants that have the potential to treat diabetes, we are interested in exploring bioactive compounds that have novel mechanisms of action. The current study isolated flavonols from *S. palustris*, primarily focusing on determining their inhibitory effects on the enzymes α-glucosidase and α-amylase. In addition, we examined the interaction between the isolated compounds and the two enzymes by conducting *in silico* studies.

2. Materials and methods

2.1. General experimental procedure

UV–vis spectra were measured on a Shidmazu UV-1800, and FTIR spectra were determined on Shimadzu, IR Prestige-21. HRMS were determined on a UHPLC Vanquish Tandem Q Exactive Plus Orbitrap, ^{1}H and ^{13}C NMR spectra were recorded with a spectrometer of Agilent DD2 system operating at 500 (^{1}H) and 125 (^{13}C) MHz, using residual and deuterated solvent peaks as reference standards. Column chromatography was performed with silica gel 60 GF_{254} (230–400 mesh, Merck). Fractions were monitored by TLC silica gel GF_{254} (Merck).

2.2. Plant material

The species' aerial parts were gathered at the Universitas Riau in Pekanbaru, Indonesia (0.539166, 101.448843) in February 2022. Prof. Fitmawati of the Department of Biology at Universitas Riau verified the plant's authenticity. A voucher specimen (No. 37/UN19.5.1.1.3–4/EP/2019) has been deposited with the Laboratory of Botany, Department of Biology, Universitas Riau.

2.3. Extraction and isolation

The air-dried and powdered aerial parts (4.0 kg) of species were extracted with methanol three times under maceration, and the crude methanol extract was partitioned in H_2O and extracted successively with *n*-hexane, dichloromethane, and ethyl acetate (Hendra et al., 2022). The ethyl acetate fraction (25 g) was separated using vacuum liquid chromatography with a silica gel column and a gradient of *n*-hexane/ethyl acetate/methanol, and five fractions (F1-5) were obtained according to the TLC monitor. All fractions were tested for α-glucose and α-amylase inhibitor activities, with fraction 5 having the highest bioactivities. Fraction 5 (1.5 g) was further purified by size-exclusion chromatography (Sephadex LH-20 in CH_3OH) and followed by flash chromatography to yield compound **1**–**5**. The isolated compounds were further elucidated their structure by using spectroscopy techniques.

2.4. In vitro α-glucosidase and α-amylase inhibition assay

A modified standard approach was used to assess the inhibitory activity of α-glucosidase. 1 mg of α-glucosidase was dissolved in 100 mL of pH 7 phosphate buffer with 200 mg of bovine serum albumin to create an enzyme solution. Before application, 1 mL of this solution was diluted 25-fold with pH 7 phosphate buffer. The reaction mixture was prepared in microplate wells with 25 l of 20 mM *p*-nitrophenyl-D-glucopyranose and 50 l of 100 mM pH 7 phosphate buffer. In DMSO, extracts, fractions, and isolated compounds were dissolved. Samples (10 µL) were combined with the reaction mixture to generate final concentrations ranging from 31.25 to 1000 µg/mL. A 1 percent acarbose (Glucobay®) solution was combined with 2 N HCl (1:1), centrifuged, and supernatant (10 µL) was added to the reaction mixture at final concentrations ranging from 0.0625 to 1 µg/mL. Blanks, controls, and samples were all performed in triplicate. After 5 min of incubation at 37 °C, 25 l enzyme solution was added and incubated for another 15 min. The enzyme process was stopped by adding 100 l of 0.1 M Na_2CO_3. Using a microplate reader spectrophotometer, absorbance was measured at 410 nm. The concentrations required for 50 percent inhibition were derived as the IC_{50} values. (El Ridhasya et al., 2020).

A range of sample concentrations (0, 50, 100, 200, and 400 µg/mL) was created. Tubes containing 100 µL of the sample were labeled S+ (with enzyme) and S- (without enzyme). In addition, tubes labeled C+ (with enzyme) and C- (without enzyme) contained 30 percent dimethyl sulfoxide (DMSO) in 0.02 M phosphate buffer (pH 6.8, 100 l) with a concentration of 30 percent. All S + and S- tubes and C + and C- tubes were inoculated with α-amylase (0.2 U/mL, 150 l), and 15 min of incubation followed at 37 degrees Celsius. After this, 250 µL of soluble starch (1 percent w/v) was added to each tube, followed by an additional 15-minute incubation. The process was stopped after one minute of boiling. Next, a part of the mixture (160 µL) was removed from each tube while preserving consistent labeling. The mixture was then heated for five minutes after adding 80 µL of 3,5-dinitrosalicylic acid (DNS). The solution was diluted with 720 µL of deionized water before measuring absorbance at 540 nm. Acarbose was the positive control in this study (standard drug). Using Equation 2, the percentage of inhibition was calculated, with C + and C- representing controls with and without the enzyme and S + and S- representing samples with and without the enzyme. The concentrations required for 50 percent inhibition were derived as the IC_{50} values.

2.5. Molecular docking

Ligands' 2D molecular structures were generated using ChemDraw Professional 19.0. Their 3D configurations were refined with MOE 2022.09.01 (Chemical Computing Group) employing the MMFF94x force field, stabilized hydrogen positions, fixed charges, and a 0.0001 gradient. These structures were stored in *.mdb format, creating a ligand database. The crystal configurations of α-glucosidase and α-amylase were sourced from https://www.rcsb.org, bearing PDB IDs 3w37 and 2QV4, respectively. These proteins were single-chained, labeled as Chain A, which was selected for docking purposes. Unwanted water molecules were stripped off using DSV 2021. The protein configuration underwent further refinement in MOE 2022.09.01 using the QuickPrep utility, integrating the CHARMM27 force field, a 0.01 gradient, and stabilized potentials. With MOE 2022.09.01, reductions were made in the H atom, alpha carbon atom, and backbone atom counts. Before molecular docking, the protein's active site had to be identified. The triangle positioning was determined, setting the posture and refinement

at 50 and 10, respectively. Following these steps, molecular docking was executed.

3. Results

3.1. Extraction and isolation

The isolation of secondary metabolites from ethyl acetate extract yielded five fractions. Further, Fraction 5 (1.5 g) was further purified by size-exclusion chromatography (Sephadex LH-20 in CH_3OH) to yield eight subfractions pooled based on TLC and $_p$-anisaldehyde staining. Subfractions 2 and 5 demonstrated their α-glucose and α-amylase inhibitor activities. Subfraction 2 was then flash chromatographed (silica, CH_3OH/CH_2Cl_2 2:8) and recrystallized to yield compound **1** (10 mg) and compound **2**. (13 mg). Subfraction 5 was then purified using silica gel flash liquid column chromatography (CH_2Cl_2/CH_3OH, 9:1 to 3:7) to yield compounds **3** (19 mg), **4** (37 mg), and **5** (15 mg). The spectroscopy data for compounds **1** – **5** are presented in supplementary information.

Stenopalustroside A (**1**), a light yellow amorphous powder (MeOH); mp 172–173 °C UV (MeOH) λ_{max} (log ε) 260 (3.15), 364 (2.01) nm; IR (KBr) v_{max} 3435, 1690, 1516 cm^{-1}; ^{1}H NMR (DMSO-d_6, 500 MHz) δ 7.96 (2H, d, J = 8.9 Hz, H-2′/6′), 7.68 (2H, d, J = 8.9 Hz, H-2′′′/6′′′), 7.50 (2H, d, J = 8.9 Hz, H-2′′′′/6′′′′), 6.89 (1H, d, J = 12.5 Hz, H-γ′′′), 6.84 (2H, d, J = 8.9 Hz, H-3′/5′), 6.75 (2H, d, J = 8.9 Hz, H-3′′′/5′′′), 6.72 (1H, d, J = 12.5 Hz, H- γ′′′), 6.69 (2H, d, J = 8.9 Hz, H-3′′′′/5′′′′), 6.32 (1H, d, J = 2.0 Hz, H-8), 6.20 (1H, d, J = 2.0 Hz, H-6), 5.88 (1H, d, J = 12.5 Hz, H-β′′′), 5.53 (1H, d, J = 12.5 Hz, H-β′′′′), 5.32 (1H, d, J = 8.0 Hz, H-1′′), 5.09 (1H, t, J = 9.0 Hz, H-3′′), 4.22 (2H, m, H-6′′), 3.61 (1H, dd, J = 9.0, 8.0 Hz, H-2′′), 3.52 (1H, m, H-5′′), 3.47 (1H, t, J = 9.0 Hz, H-4′′); ^{13}C NMR (DMSO-d_6, 125 MHz) δ 179.2 (C, C-4), 167.9 (C, C-α′′′), 167.7 (C, C-α′′′′), 166.4 (C, C-7), 163.1 (C, C-5), 161.5 (C, C-4′), 160.0 (C, C-4′′), 160.5 (C, C-4′′′), 159.4 (C, C-2), 158.5 (C, C-9), 145.5 (CH, C-γ′′′′), 144.9 (CH, C-γ′′′), 135.1 (C, C-3), 133,7 (CH, C-2′′′/6′′), 133.5 (CH, C-2′′′′/6′′′′), 132 (CH, C-2′/6′), 127.6 (C, C-1′′), 127.6 (C, C-1′′′) 122.7 (C, C-1′), 116.8 (CH, C-β′′′), 116.3 (CH, C-β′′′′), 116.1 (CH, C-3′/5′), 115.5 (CH, C-3′′′/5′′′), 115.2 (CH, C-3′′′′/5′′′′), 105.6 (C, C-10), 103.8 (C, C-1′′), 100.1 (CH, C-6), 94.9 (CH, C-8), 78.3 (CH, C-3′′), 75.5 (CH, C-5′′), 74.0 (CH, C-2′′), 70.0 (CH, C-4′′), 63.8 (CH_2, C-6′′); HRMS (ESI-TOF) m/z 763.1628 $[M + Na]^+$ (calcd for $C_{39}H_{32}O_{15}Na^+$, 763.1639).

Tiliroside (**2**), yellow amorphous powder (MeOH); mp 258–260 °C, UV (MeOH) λmax (log ε) 262 (4.25), 360 (2.76) nm; IR (KBr) vmax 3311, 1660, 1506 cm-1; 1H NMR (DMSO-d_6, 500 MHz) 8.06 (d, J = 8.3 Hz, 2H, H2′/6′), 7.40 (d, J = 15.8 Hz, 1H, H3′′), 7.31 (d, J = 8.1 Hz, 2H, H2′′′′/6′′′′), 6.84 (d, J = 8.3 Hz, 2H, H3′′′′/5′′′′), 6.81 (d, J = 2.4 Hz, 2H, H3′/5′), 6.80 (d, J = 8.1 Hz, 1H, H2′), 6.32 (s, 1H, H8), 6.14 (s, 1H, H6), 6.07 (d, J = 15.9 Hz, 1H, H2′′), 5.24 (d, J = 6.7 Hz, 1H, H1′′), 4.18 (dd, J = 11.5, 1.2 Hz, 1H, H6′′a), 4.30 (dd, J = 11.9, 6.1 Hz, 1H, H6′′b), 3.48 (dd, J = 7.0, 8.9 Hz, 1H, H2′′), 3.42 (ddd, J = 8.9, 6.1, 1.2 Hz, 1H, H5′′), 3.35 (dd, J = 9.0, 8.0 Hz, 1H, H4′′), 3.22 (dd, J = 9.0, 9.5 Hz, 1H, H3′′); ^{13}C NMR (DMSO-d_6, 125 MHz) 179.7 (C4), 168.8 (C1′′), 165.9 (C7), 163.8 (C5), 161.6 (C2), 158.4 (C8a), 146.8 (C4′), 146.6 (C3′′), 142.2 (C4′′′), 132.4 (C3), 132.3 (C2′/6′), 131.2 (C2′′′/6′′′), 126.1 (C1′′′), 123.0 (C1′), 116.6 (C3′′′/C8′′), 116.3 (C3′/5′), 114.9 (C2′′), 105.7 (C4a), 104.1 (C1′′), 100.2 (C6), 95.0 (C8), 78.2 (C3′′), 75.9 (C2′′), 75.8 (C5′′), 71.9 (C4′′), 64.5 (C6′′).

Kaempferol (**3**), a light yellow amorphous powder (MeOH); mp 276–278 °C; UV (MeOH) λ_{max} (log ε) 266 (4.55), 368 (2.61) nm; IR (KBr) v_{max} 3311, 1660, 1506 cm^{-1}; ^{1}H NMR (DMSO-d_6, 500 MHz) δ 12.4 (1H, s, 5-OH), 8.03 (2H, d, J = 9.0 Hz, H-3′/5′), 6.91 (2H, d, J = 9.0 Hz, H-2′/6′), 6.39 (1H, d, J = 2.3 Hz, H-8), 6.17 (1H, d, J = 2.3 Hz, H-6); ^{13}C NMR (DMSO-d_6, 125 MHz) δ 176.3 (C carbonyl, C-4), 164.3 (C, C-7), 161.2 (C, C-5), 156.6 (C, C-9), 159.6 (C, C-4′), 147.3 (C, C-2), 136.1 (C, C-3), 129.9 (C, C-3′/5′), 122.4 (C, C-1′), 115.9 (CH, C-2′/6′), 103.4 (C, C-10), 93.8 (CH, C-8), 98.6 (CH, C-6).

Quercetin (**4**), a light yellow amorphous powder (MeOH); mp 224–226 °C; UV (MeOH) λ_{max} (log ε) 256 (4.25), 370 (2.41) nm; IR (KBr) v_{max} 3007, 2827, 1514, 1170 cm^{-1}; ^{1}H NMR (DMSO-d_6, 500 MHz) δ 12.4 (1H, s, 5-OH), 9.29 (1H, s, 3-OH), 7.53 (1H, d, J = 2.0 Hz, H-2′), 7.53 (1H, dd, J = 8.1 Hz,; J = 2.0 Hz, H-6′), 6.83 (1H, d, J = 8.1 Hz, H-5′), 6.39 (1H, d, J = 2.3 Hz, H-8), 6.17 (1H, d, J = 2.3 Hz, H-6); ^{13}C NMR (DMSO-d_6, 125 MHz) δ 176.3 (C carbonyl, C-4), 164.3 (C, C-7), 161.2 (C, C-5), 156.6 (C, C-9), 148.2 (C, C-4′), 145.5 (C, C-3′), 147.3 (C, C-2), 122.4 (C, C-1′), 120.4 (CH, C-6′), 116.1 (CH, C-5′), 115.5 (CH, C-2′), 103.46 (C, C-10), 93.8 (C, C-8), 98.6 (C, C-6).

Rutin (**5**), a yellow amorphous powder (MeOH); mp 240–242 °C; UV (MeOH) λ_{max} (log ε) 258 (5.22), 358 (3.71) nm; IR (KBr) v_{max} 3070, 1504, 806 cm^{-1}; ^{1}H NMR (DMSO-d_6, 500 MHz) δ ^{1}H NMR (DMSO-d_6, 500 MHz) δ 12.4 (1H, s, 5-OH), 9.29 (1H, s, 3-OH), 7.53 (1H, d, J = 2.0 Hz, H-2′), 7.53 (1H, dd, J = 8.1 Hz,; J = 2.0 Hz, H-6′), 6.83 (1H, d, J = 8.1 Hz, H-5′), 6.39 (1H, d, J = 2.3 Hz, H-8), 6.17 (1H, d, J = 2.3 Hz, H-6), 5.11 (H1, d, J = 7.0 Hz, H-1′′), 5.08 (H1, s, H-1′′′), 3.80 (1H, dd, J = 8.4, 8.0 Hz, H-6a′′), 3.62 (1H, dd, J = 8.4 Hz, 8.0 Hz, H-2′′), 3.51 (1H, dd, J = 8.4 Hz, 8.0 Hz, H-3′′), 3.44 (1H, dd, J = 8.4 Hz, 8.0 Hz, H-5′′), 3.43–3.41 (1H, m, H-2′′), 3.40 (1H, t, J = 8.0 Hz, H-3′′), 3.37 (1H, dd, J = 8.4 Hz, 8.0 Hz, H-6$_b$′′), 3.32–3.33 (1H, m, H-5′′), 3.27 (1H, dd, J = 8.4 Hz, 8.0 Hz, H-4′′), 3.24 (1H, dd, J = 8.4 Hz, 8.0 Hz, H-4′′), 1.11 (3H, s, H-6′′; ^{13}C NMR (DMSO-d_6, 125 MHz) δ 197.7 (C, CO ketone), 165.3 (C, C-7), 163.4 (C, C-5), 163.2 (C, C-9), 158.3 (C, C-4′), 129.1 (C, C-1′), 128.9 (CH, C-2′/6′), 115.7 (CH, C-3′/5′), 103.7 (C, C-10), 100.8 (CH, C-1′′), 97.8 (CH, C-1′′′), 96.7 (CH, C-6), 95.6 (CH, C-8), 79.08 (CH, C-2), 77.6 (CH, C-3′′), 77.4 (CH, C-5′′), 76.5 (CH, C-2′′), 72.3 (CH, C-3′′′), 70.9 (CH, C-2′′′), 70.8 (CH, C-3′′′), 70.03 (CH, C-4′′), 68.0 (CH, C-5′′′), 60.89 (CH_2, C-6′′), 42.6 (CH_2, C-3), 18.5 (CH_3, C-6′′′).

3.2. In vitro α-glucosidase and α-amylase inhibition assay

Prior to isolating compounds **1**–**5**, an exhaustive evaluation was performed on all extracts to determine their potential to inhibit α-glucosidase and α-amylase (as depicted in Table 1). The results presented in Table 1 demonstrate that ethyl acetate extract inhibits both enzymes significantly with IC_{50} value of 141.3 μg/mL for α-glucosidase, and 312.3 μg/mL for α-amylase, with dichloromethane extract following suit in terms of effectiveness. Nonetheless, it is notable that dichloromethane extracts exhibited limited α-amylase inhibition, indicating a more selective inhibition profile for this particular enzyme. The findings led to the subsequent purification of the compound within the ethyl acetate extract, which separated the compound into five distinct fractions. All five fractions were subjected to enzyme inhibition assays to determine their inhibitory potential. The results demonstrated that fraction 5 exhibited the most potent inhibition activity against both enzymes with IC_{50} value of 57.4 μg/mL for α-glucosidase, and 143.2 μg/

Table 1
In vitro α-glucosidase and α-amylase inhibition assay of extracts, fractions, and compound 1–5.

Sample	IC_{50} (μg/mL)	
	α-glucosidase	α-amylase
n-hexane extract	> 1000	> 1000
Dichloromethane extract	342.2 ± 2.02	> 1000
Ethyl acetate extract	141.3 ± 1.14	312.3 ± 1.23
Water extract	> 1000	> 1000
Fraction 1	> 500	> 500
Fraction 2	> 500	> 500
Fraction 3	> 500	> 500
Fraction 4	> 500	> 500
Fraction 5	57.4 ± 0.54	143.2 ± 1.76
1	201.2 ± 1.52	> 250
2	63.8 ± 0.63	180.6 ± 2.04
3	56.4 ± 0.13	135.2 ± 1.84
4	43.6 ± 0.32	118.4 ± 1.38
5	47.2 ± 0.11	177.2 ± 2.01
Acarbose	114.6 ± 0.10	98.32 ± 0.54

mL for α-amylase, surpassing the inhibitory effects of the other fractions (Table 1). As a result of this encouraging result, a more thorough purification procedure was carried out on fraction 5, isolating the five compounds (**1**–**5**) described previously.

3.3. Molecular docking

An *in silico* molecular docking experiment was carried out in this study to determine the binding affinity and modes of compounds **1**–**5** with the active sites of target enzymes α-glucosidase and α-amylase. The molecular docking results of compounds **1**–**5** and acarbose with α-glucosidase (PDB ID: 3w37) and α-amylase (PDB ID: 2QV4) are shown in Tables 2 and 3, respectively. Figs. 2 and 3 also show the spatial orientation of compounds **1**–**5** and acarbose in relation to α-glucosidase and α-amylase, as well as their ligand–protein interactions.

4. Discussion

The *Stenochlaena palustris* (Burm. f.) Bedd, a popular form of edible fern found in Southeast Asia, is regarded to be high in nutrients and beneficial to human health, including aiding in blood glucose control and lowering the risk of diabetes. It is hypothesized that several minerals and antioxidants could explain its positive effects and that it is used in traditional medicinal practice (Ndanusa et al., 2020). In this work, we investigated and reported the α-glucosidase and α-amylase inhibition of the species and the secondary metabolites responsible for these biological activities based on a bioassay-guided approach. The species were extracted using various organic solvents to achieve *n*-hexane, dichloromethane, ethyl acetate, and water.

The extracts were employed for α-glucosidase and α-amylase inhibition assay, and the results revealed that the ethyl acetate extract showed potential biological activity. Furthermore, the ethyl acetate extract was purified to obtain the secondary metabolites using a bioassay-guided approach using successive chromatographic works. After their molecular structure elucidation, five compounds were successfully isolated and purified using spectroscopic and spectrometric techniques. Compound 3 was isolated as yellow amorphous powder, and its ^{1}H NMR spectrum exhibited two coupled doublets at δ 6.17 and 6.39, featuring a coupling constant (J = 2.3 Hz). These characteristic resonances were attributed to the *meta*-relationship of the H-6 and H-8 protons within the ring A of the flavonoid derivative. Additionally, the chemical shifts provided compelling evidence for a 5,7-dihydroxy substitution pattern on ring A. Notably, the presence of a 1,4 substituted benzene ring (δ_H 8.03, 2H, d, J = 9.0 Hz and δ_H 6.91, 2H, d, J = 9.0 Hz) was ascribed to the B-ring. The congruence of this information with established literature unequivocally supported the identification of the compound as kaempferol (**3**) (Hendra and Keller, 2016).

Compound **1** emerged as a yellow amorphous powder. High-resolution mass spectrometry (HRMS) of Compound 1 revealed a prominent *m/z* value of 763.1628, corresponding to a sodium adduct ion $[M + Na]^+$ attributed to $C_{39}H_{32}O_{15}Na^+$. Within the ^{1}H NMR spectrum, kaempferol (**3**) was evident, adorned with an additional sugar moiety as a β-glucopyranose. Notably, in the HMBC spectrum, a long correlation between C-3 (δ 132.4) and the anomeric proton (δ 5.532, 1H, d, J = 8.0 Hz), pinpointing the glycosylation site at the 3-OH of **3**. Furthermore, the assemblage of two 1,4-substituted aromatic rings, in conjunction with the discernible presence of two sets of doublet protons associated with double bond positions (J = 12.5 Hz), as well as the distinct peaks at δ 167.9 and 167.7 denoting ester carbonyl carbons, collectively implied the occurrence of two *cis-p*-coumaroyl moieties. The attachment of these acyl coumaroyl substituents to the 3′–OH and 6′–OH positions was decisively substantiated by the conspicuous downfield shifts observed in the glucose unit, with H-3′ (δ 5.09) and H-6′ (δ 4.22, 2H) bearing to these linkages. Henceforth, the comprehensive elucidation of the structural facets coalesced to confirm the distinct identity of compound **1** as stenoplaustroside A, an assertion reinforced by comparison with data documented by Liu et al. (1999).

Furthermore, the examination of the ^{1}H NMR spectrum of compound **2** unveiled the presence of **3**, identifying a sugar moiety in the form of β-glucopyranose and detecting *cis-p*-coumaroyl moieties. The attachment of these acyl coumaroyl substituents to the 6′–OH positions was unequivocally corroborated by the strikingly observable downfield shifts evident within the glucose unit. This was most evident in the resonances of H-6′ (δ 4.18, dd, J = 11.5, 1.2 Hz, H6′a and δ 4.30, dd, J = 11.9, 6.1 Hz, H6′b), which served as compelling indicators of these linkages. Based on these data and in comparison with the available literature, compound **2** is designated as tiliroside (Liu et al., 1999, Hendra and Keller, 2017). Furthermore, unique paired doublets at 6.17 and 6.39, defined by a coupling constant (J = 2.3 Hz), were identified in the 1H NMR spectrum of compound 4. These distinct resonances were linked to the *meta*-relationship of the flavonoid derivative's H-6 and H-8 protons within ring A. Notably, the presence of a 1,3,4-substituted benzene ring (δ_H 7.53, d, J = 2.0 Hz; δ_H 7.53, dd, J = 8.1 Hz, J = 2.0 Hz; δ_H 6.83 d, J = 8.1 Hz) was reliably identified as the B-ring, leading to the chemical being identified as quercetin. Simultaneously, analysis of compound **5** revealed not only the presence of compound **4** but also the addition of a sugar moiety in the form of rutinose. The HMBC spectrum also revealed a significant correlation extending between C-3 (δ_C 132.4) and the anomeric proton (δ_H 5.53, 1H, d, J = 8.0 Hz), indicating the site of glycosidation at compound **4**′s 3-OH position. In summary, rutin (**5**) emerged from **4** after adding a rutinose sugar moiety. The precision of the analysis and the solidification of compound identifications were highlighted by a rigorous comparison with previously published data, confirming the accuracy of these findings (Hendra and Keller, 2016). Compounds **1** and **2** have previously been reported from the leaves of this species in Papua New Guinea (Liu et al., 1999). Even though compounds **3**–**5** are common flavonols found in plants and foods (Liga et al., 2023), they are reported for the first time from this species (Fig. 1).

Table 2
Docking results of 1–5 for PDB ID 3w37.

Compound	S (kcal/mol)	RMSD	H bond	Hydrophobic	van der Walls	The others interaction	Binding Factor
Acarbose	**−4,7441**	**1,8116**	**Asp357, Asp469, Arg552, Asp232**	**Lys506**	**Asp568**	**Ser497, Ala602, Trp432, Phe601, Trp329, His626, Ile396, Trp467, Ile233, Phe476, Tyr243, Ala234,**	**18**
1	−8.1472	2.0656	Asp630	**Ala234, Lys506**	**Asp232**	**Trp329, Ala602,** Ala628, **Phe601,** Thr631**, Phe476, Trp432, Tyr243,** Phe236, **Ile233, Ser497,** Asn237, Gly498, Leu240	11
2	−6.7292	1.4117	Gly721, Asp785, Glu756	Arg720	Asp684	Ser736, Asn722, His786, Ser784, His755, Val787, Phe680, Pro683, Thr681,	–
3	−5.3615	1.0615	Leu369, Thr368	Arg456, Arg412	–	Leu376, Ile460, Phe457, Phe367	–
4	−5.0772	0.8868	**Trp329, Asp357, Asp568**	**Arg552**	**Asp232, Asp469**	**Phe476, Trp432, His626,** Ile358**, Ile396, Trp467,** Met470, **Phe601, Ala234, Ala602**	14
5	−6.9946	1.6292	**Ala234**	**Arg552, Lys506**	Asp568, **Asp232**	Ile477, Met470, **Phe476, Trp432, Tyr243,** Asn237, Phe236, **Ser497, Ile233**	9

Table 3
Docking results of 1–5 for PDB ID 2QV4.

Compound	S (kcal/mol)	RMSD	H bond	Hydrophobic	van der Walls	The others interaction	Binding Factor
Acarbose	**−8.1445**	**1.4846**	**Asp197, Glu233, Lys200**	–	**Asp300, Glu240**	**Ile235, Leu165, Leu162, Gly164, Thr163, Tyr151, Pro241, His305, Gly306, Trp59, Tyr62, Trp58, His101**	**18**
1	−9.4254	1.8807	**Asp197,** Ala307, **Thr163**	Gly308, **Lys200**	**Glu240**	Val98, **Tyr62, His101, Ile235, Trp59,** Gln63, Val107, Ala106, **Gly164, Leu165,** Gly309, Gly304, **Gly306, His305**	12
2	−8.9655	2.1911	**Trp59, Asp300**	**Lys200**	**Asp197, Glu233**	**Tyr62, Trp58,** Gln63, **Gly164,** Ala106, **Thr163, Leu165, Leu162,** Val157, His201, **Tyr151, Pro241, Ile235, Gly306, His305**	16
3	−5.8343	0.8721	**Asp197**	**Lys200**	**Asp300, Glu233**	**Leu165, Leu162,** His201, **Ile235,** Ala198, **His101, Tyr62, Trp59**	10
4	−6.3228	0.7311	**Asp197**	**Lys200**	**Asp300, Glu233**	**Leu165, Leu162,** His201, **Ile235,** Ala198, **His101, Trp58, Tyr62, Trp59**	11
5	−8,1960	1,2263	**Lys200**	–	**Asp300, Glu233, Glu240**	**Tyr62, Trp58, Leu165, His101, Leu162, Ile235,** Ala198, His201, Ser199, Val157, **Pro241, Tyr151, His305, Trp59**	14

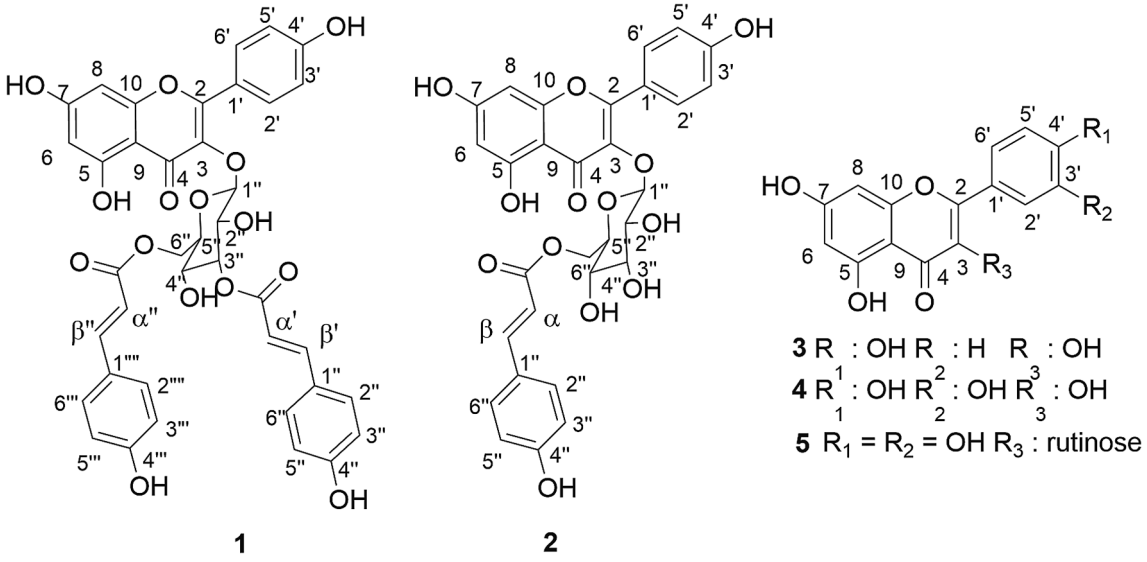

Fig. 1. Molecular structures of compounds isolated from *S. palustris* (Burm.f.) Bedd.

Additionally, Table 1 comprehensively overviews the five isolated compounds' diverse activities of α-glucosidase and α-amylase inhibitions. Each of these isolated compounds inhibited α-glucosidase more strongly than it inhibited α-amylase. Compound **4** stood out, inhibiting the α-glucosidase enzyme significantly more than the other compounds and outperforming acarbose, a known positive control. Similarly, Compound **4** demonstrated greater efficacy in inhibiting α-amylase than the other compounds, although at a lower activity level than acarbose. Furthermore, the inhibitory potential of compound **1** is investigated in this study. The results showed a limited inhibitory capacity against both enzymes, with IC_{50} values of 200 μg/mL and greater than 250 μg/mL. Notably, the inhibitory efficacy of compound **1** highlighted here is a novel discovery encompassing both enzymes, providing valuable insights into the field of enzymatic inhibition.

Our results indicate that the isolated flavonols from the investigated species exhibit distinct inhibitory activities against α-glucosidase and α-amylase enzymes. Flavonols, a subclass of flavonoids, have been identified as biologically active compounds capable of inhibiting these critical enzymes in carbohydrate metabolism. As supported by previous research, the molecular structure of flavonoids, including the position and number of hydroxyl (OH) groups, plays a crucial role in modulating this inhibitory effect (Proença et al., 2017). In a 2017 study conducted by Proenca et al., the IC_{50} values for kaempferol and quercetin indicated that kaempferol had approximately half the inhibitory potency of quercetin. This indicates that flavonols with dihydroxy substitutions at the 2′ and 4′ or 3′ and 4′ positions of the B-ring inhibit alpha-glucosidase more effectively than those with a single hydroxy substitution at the 3′ or 4′ position (Proença et al., 2017, Şöhretoğlu and Sari, 2020). In addition, a 2018 study by Sohretoglu et al. emphasized that the sugar substitution at the C3-OH position on the C-ring of flavonols reduced the enzyme-inhibiting effect. Intriguingly, it was observed that the addition of galloyl groups to these sugar units increased their inhibitory activity (Şöhretoğlu et al., 2018). Furthermore, the inhibitory effects of flavonols on α-amylase follow a similar pattern to that of α-glucosidase. Notably, a C2-C3 double bond in the C-ring increases the inhibitory activity. This structural characteristic contributes positively to the enzyme-substrate interaction, possibly resulting in more efficient enzyme inhibition (Proença et al., 2019). Furthermore, Compound **2**, derived from *Elaeagnus angustifolia* L., exhibited substantial α-glucosidase inhibitory activity and showcased a noteworthy potency, as indicated by its IC_{50} value of 2128 ± 63 μM. This discovery is especially significant in light of the potential therapeutic uses of these inhibitors in the treatment of postprandial hyperglycemia and other metabolic disorders (Yuca et al., 2021).

This study also includes the results of the compounds' *in silico* analyses, which support our findings. *In silico* approaches, encompassing molecular docking and various computational techniques, play a pivotal role in drug discovery. These tools empower scientists to pinpoint and prioritize potential lead compounds, refine their characteristics, and enhance the prospects of formulating efficacious and safe medications

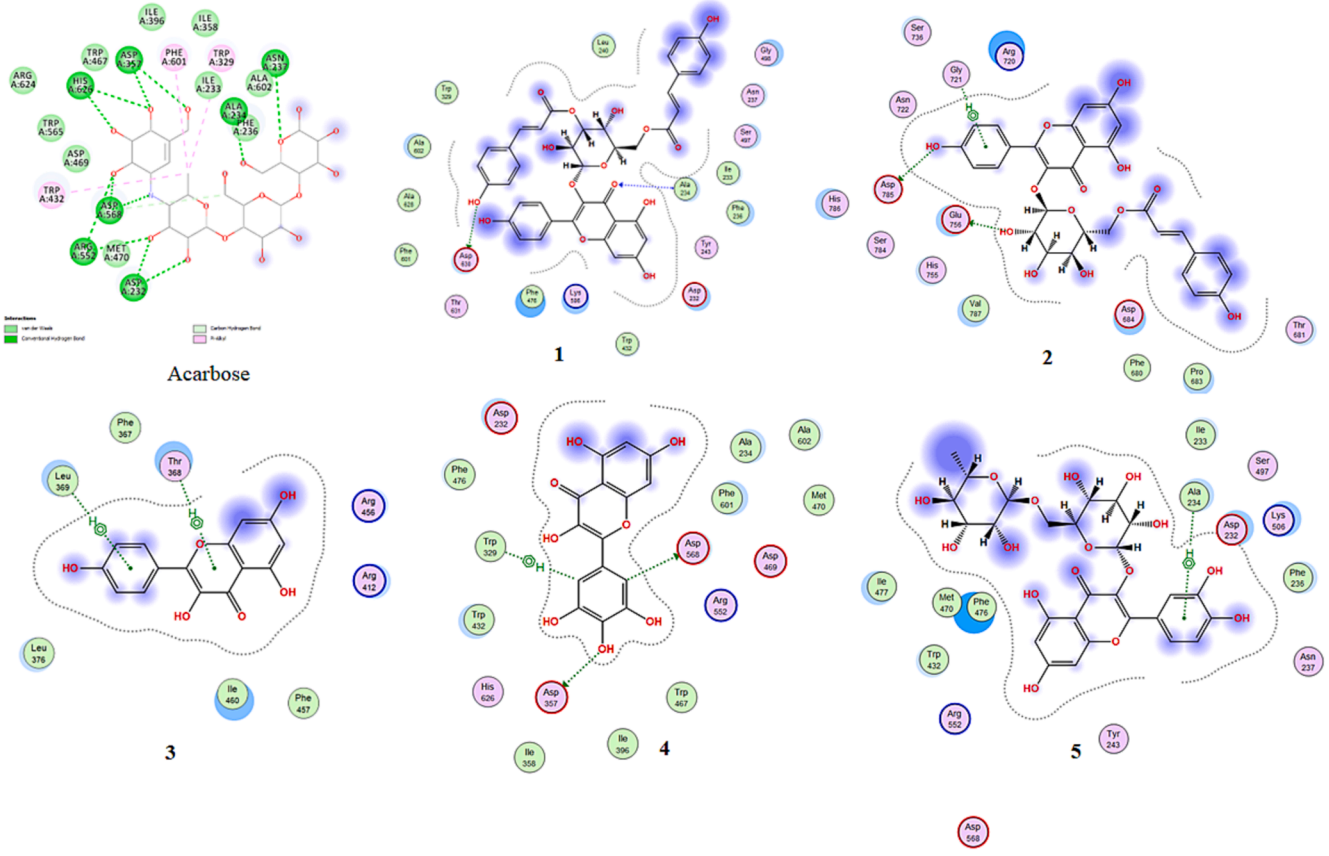

Fig. 2. Spatial arrangement of acarbose, 1–5 toward α-glucosidase (PDB ID: 3w37).

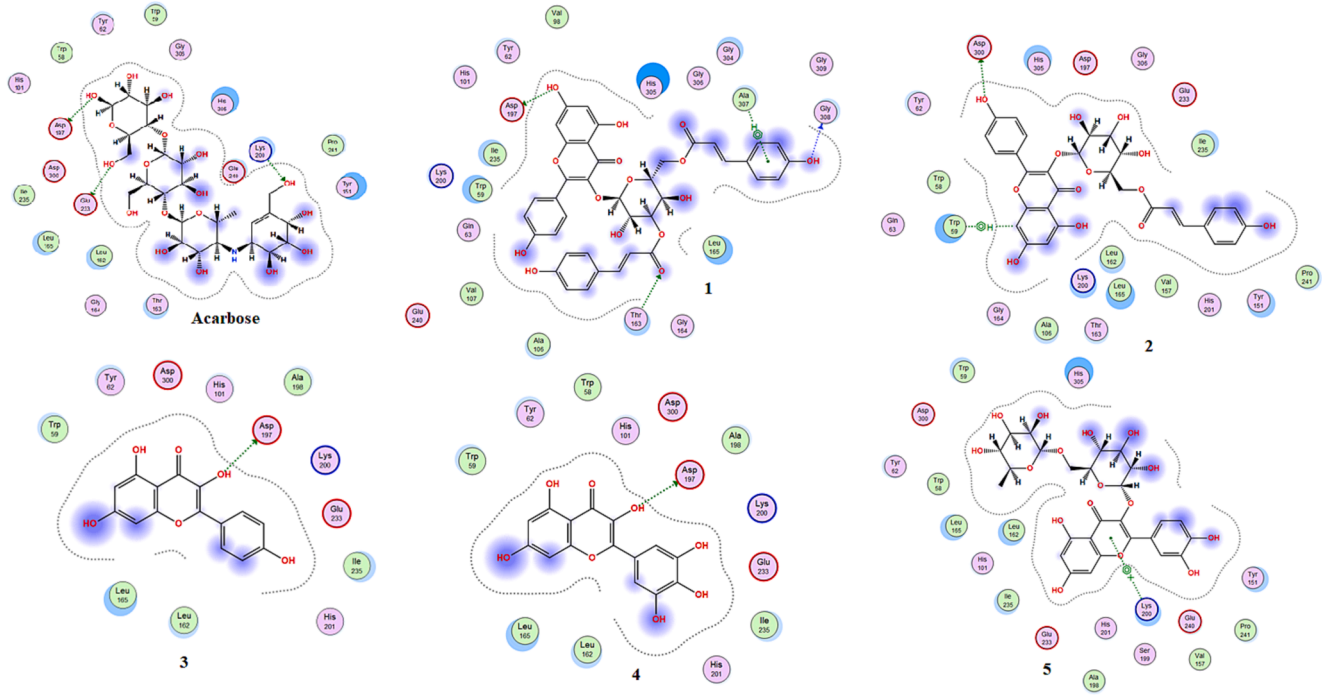

Fig. 3. Spatial arrangement of acarbose, 1–5 toward α-amylase and their ligand–protein interaction (PDB ID: 2QV4).

(Frimayanti et al., 2023). Molecular docking is a robust computational technique offering insights into ligand-receptor interactions. This method, vital to contemporary drug discovery, aids in recognizing, fine-tuning, and understanding prospective drug molecules (Santoso et al., 2022).

To comprehend the interactions between ligands and protein binding

sites, the compounds were docked into the protein targets α-glucosidase and α-amylase, which were obtained from https://www.rcsb.org with PDB IDs 3w37 and 2QV4, respectively. The results of the docking analysis for these ligands are presented in Table 2. The positive control, Acarbose, recorded the most favorable binding free energy of −4.7441 kcal/mol per the docking findings. It forms hydrogen bonds with amino acids like Asp357, Asp469, Arg552, and Asp232. Moreover, a van der Waals interaction was observed between doxorubicin and the amino acid Asp568. Hydrophobic interactions were also noticed between acarbose and the Lys506 amino acid. Fig. 2 illustrates acarbose's spatial configuration. Compound **1** has a binding free energy of −8.1472 kcal/mol. A notable hydrogen bond is formed with the amino acid Asp630. This particular amino acid bond differs from that in the positive control, suggesting compound **1** inhibits α-glucosidase differently. Significant amino acid interactions were identified through van der Waals contacts with Asp232. Despite sharing amino acid sequences with the positive control, these molecules have an RMSD greater than two, hinting that α-glucosidase might resist inhibition by Compound **1**. Its spatial configuration is portrayed in Fig. 2.

Moreover, compound **5** showcases binding free energies less favorable than acarbose. Interaction pathways include hydrogen bonds formed between carbonyl groups and the amino acid residue Ala234, along with van der Waals interactions involving Asp232 and Asp568. Hydrophobic bonds were also established with amino acid residues Arg552 and Lys506. Fig. 2 represents its spatial positioning. Furthermore, compound **4** presents a binding free energy of −5.0772 kcal/mol. Its energy binding was found to be less harmful compared to acarbose. Docking visualizations revealed three hydrogen bonds: a hydroxyl group and Asp357, a benzene ring with Asp568, and Trp329. Compound **4** also showcased van der Waals contacts and other associations with various amino acid residues. Notably, the interactions align with those seen for acarbose, making compound **4** a likely active agent. Its interaction with the protein is depicted in Fig. 2. Contrastingly, Compounds **2** and **3**, based on the docking results, failed to exhibit analogous amino acid interactions as the positive control, deeming them unsuitable as potential α-glucosidase inhibitors.

Furthermore, the compounds and acarbose were docked into the α-amylase protein targets. According to the docking data in Table 3, acarbose was used as a positive control, with a binding free energy value of −8.1445 kcal/mol and an RMSD value of 1.4846. Through the hydroxyl group and the amino acid residues Asp197, Glu233, and Lys200, acarbose was able to form three hydrogen bonds with protein. Acarbose's van der Waals interaction with Asp300 and Glu240 was investigated. Binding with amino acid residues is essential in this case because these amino acid residues are involved in the breakdown of polyproteins required for viral replication. Fig. 3 depicts the spatial arrangement of acarbose.

Compounds **1**, **2**, and **3** interact with the protein active site with binding free energies of −9.4254, −8.9655, and −5.8343 kcal/mol in which higher negative binding free energy becomes more stable, and the reaction occurs independently (Ahmed et al., 2022). Furthermore, the negative binding free energy value facilitates a ligand's ability to bind to the protein's active site. In this case, even though compounds **1** and **2** have a lower binding free energy value than acarbose, they have a higher RMSD value. As a result, these compounds may become inactive. Fig. 3 depicts the spatial arrangement of compounds **1**, **2**, and **3**. On the other hand, compounds **4** and **5** interact with the active site, producing binding free energies of −6.3228 and −8.1960 kcal/mol. Furthermore, these compounds had a higher binding factor. Compound **4** demonstrated hydrogen bond interaction between ligand hydroxyl groups and amino acid residue Asp197; this compound also investigated van der Waals interaction via amino acids Asp300 and Glu233. The amino acid interactions that occur are identical to the amino acid interactions that occur in the positive control. As a result, compound **4** may become an active agent. Compound **5** was thought to be active because it formed a hydrogen bond with the same amino acid as positive control Lys200. Furthermore, this compound is bound to the same amino acid as the positive control via a hydrophobic interaction with the amino acid residues Asp300 and Glu240. Compounds **4** and **5** are arranged in their spatial configuration, as shown in Fig. 3.

5. Conclusions

A phytochemical study of the ethyl acetate extract from *S. palustris* led to the extraction of five flavonols (stenopalustroside A (**1**), tiliroside (**2**), kaempferol (**3**), quercetin (**4**), and rutin (**5**)). These compounds demonstrated diverse levels of inhibition against α-glucosidase and α-amylase. Strikingly, Compound **4** emerged as the most potent inhibitor of these enzymes. *In silico* analyses, we suggested that the amino acid interactions observed in compounds **4** and **5** mirrored those in the positive control. Consequently, this similarity might render these compounds as effective agents.

CRediT authorship contribution statement

Rudi Hendra: Conceptualization, Methodology, Validation, Formal analysis, Investigation, Resources, Data curation, Writing – original draft, Writing – review & editing, Visualization. **Monika Kerry Army:** Formal analysis, Investigation, Data curation, Visualization. **Neni Frimayanti:** Validation, Investigation, Data curation, Writing – original draft. **Hilwan Yuda Teruna:** Conceptualization, Methodology, Formal analysis, Investigation, Writing – original draft, Writing – review & editing, Visualization. **Rizky Abdulah:** Conceptualization, Methodology, Resources, Writing – review & editing. **Ari Satia Nugraha:** Conceptualization, Methodology, Validation, Formal analysis, Investigation, Writing – original draft, Writing – review & editing.

Declaration of competing interest

The authors declare that they have no known competing financial interests or personal relationships that could have appeared to influence the work reported in this paper.

Acknowledgment

The authors extend their gratitude to the Centre of Research and Community Development at the University of Riau and the Ministry of Research, Technology, and Higher Education of the Republic of Indonesia for their invaluable support. This research was funded through Grant No. 11320/UN19.5.1.3/AL.04/2023.

Appendix A. Supplementary material

Supplementary data to this article can be found online at https://doi.org/10.1016/j.jsps.2023.101940.

References

Ahmed, S., Ali, M.C., Ruma, R.A., et al., 2022. Molecular docking and dynamics simulation of natural compounds from betel leaves (Piper betle L.) for investigating the potential inhibition of alpha-amylase and alpha-glucosidase of type 2 diabetes. Molecules 27, 4526. https://doi.org/10.3390/molecules27144526.

Chai, T.-T., Kwek, M.-T., Ong, H.-C., et al., 2015. Water fraction of edible medicinal fern Stenochlaena palustris is a potent α-glucosidase inhibitor with concurrent antioxidant activity. Food Chem. 186, 26–31. https://doi.org/10.1016/j.foodchem.2014.12.099.

Chang, T.-C., Chiang, H., Lai, Y.-H., et al., 2019. Helminthostachys zeylanica alleviates hepatic steatosis and insulin resistance in diet-induced obese mice. BMC Complement. Altern. Med. 19, 1–11. https://doi.org/10.1186/s12906-019-2782-3.

Chen, S., Yong, T., Xiao, C., et al., 2018. Pyrrole alkaloids and ergosterols from Grifola frondosa exert anti-α-glucosidase and anti-proliferative activities. J. Funct. Foods 43, 196–205. https://doi.org/10.1016/j.jff.2018.02.007.

Dysted, M. P., B. Esztergalyos, S. Gautam, et al., 2021. IDF Diabetes Atlas. E. J. Boyko, D. J. Magliano, S. Karuranga et al. Brussel, Belgium, International Diabetes Federation.

El Ridhasya, F., Rahim, N., Almurdani, M., et al., 2020. Antidiabetic constituents from Helminthostachys zeylanica (L) hook (Ophioglossaceae). Pharmacogn. J. 12 https://doi.org/10.5530/pj.2020.12.33.

Frimayanti, N., Ikhtiarudin, I., Septama, A.W., et al., 2023. Synthesis, in silico and structural insight of flavonol derivative compounds as new competitive dengue NS2B/NS3 protease inhibitor. J. Res. Pharm. 27 https://doi.org/10.29228/jrp.406.

Hendra, R., Keller, P.A., 2016. Flowers in Australia: phytochemical studies on the Illawarra flame tree and Alstonville. Aust. J. Chem. 69, 925–927. https://doi.org/10.1071/CH16058.

Hendra, R., Keller, P.A., 2017. Phytochemical studies on two Australian Anigozanthos plant species. J. Nat. Prod. 80, 2141–2145. https://doi.org/10.1021/acs.jnatprod.7b00063.

Hendra, R., Khodijah, R., Almurdani, M., et al., 2022. Free radical scavenging, anti-infectious, and toxicity activities from Stenochlaena palustris (Burm. f.) Bedd. Extracts. Adv. Pharmacol. Pharm. Sci. 2022, 1–8. https://doi.org/10.1155/2022/5729217.

Karakaya, S., Gözcü, S., Güvenalp, Z., et al., 2018. The α-amylase and α-glucosidase inhibitory activities of the dichloromethane extracts and constituents of Ferulago bracteata roots. Pharm. Biol. 56, 18–24.

Kim, K.-T., Rioux, L.-E., Turgeon, S.L., 2014. Alpha-amylase and alpha-glucosidase inhibition is differentially modulated by fucoidan obtained from Fucus vesiculosus and Ascophyllum nodosum. Phytochemistry 98, 27–33. https://doi.org/10.1016/j.phytochem.2013.12.003.

Liga, S., Paul, C., Péter, F., 2023. Flavonoids: Overview of biosynthesis, biological activity, and current extraction techniques. Plants 12, 2732. https://doi.org/10.3390/plants12142732.

Liu, H., Orjala, J., Sticher, O., et al., 1999. Acylated flavonol glycosides from leaves of Stenochlaena palustris. J. Nat. Prod. 62, 70–75. https://doi.org/10.1021/np980179f.

Ndanusa, A., Cicuzza, D., Siddique, M., 2020. Analysis of the phytochemical contents and anti-oxidative properties of Stenochlaena palustris. Int. Food Res. J. 27, 798–804.

Neeland, I. J. and K. V. Patel, 2019. Diabetes: Key markers of injury and prognosis. Biomarkers in cardiovascular disease, Elsevier: 41-51.

Proença, C., Freitas, M., Ribeiro, D., et al., 2017. α-Glucosidase inhibition by flavonoids: an in vitro and in silico structure–activity relationship study. J. Enzyme Inhib. Med. Chem. 32, 1216–1228. https://doi.org/10.1080/14756366.2017.1368503.

Proença, C., Freitas, M., Ribeiro, D., et al., 2019. Evaluation of a flavonoids library for inhibition of pancreatic α-amylase towards a structure–activity relationship. J. Enzyme Inhib. Med. Chem. 34, 577–588. https://doi.org/10.1080/14756366.2018.1558221.

Rosak, C. and G. Mertes, 2012. Critical evaluation of the role of acarbose in the treatment of diabetes: patient considerations. Diabetes, metabolic syndrome and obesity: targets and therapy. 357-367. Doi: https://doi.org/10.2147/DMSO.S28340.

Santoso, M., Ong, L.L., Aijijiyah, N.P., et al., 2022. Synthesis, α-glucosidase inhibition, α-amylase inhibition, and molecular docking studies of 3, 3-di (indolyl) indolin-2-ones. Heliyon 8. https://doi.org/10.1016/j.heliyon.2022.e09045.

Şöhretoğlu, D., Sari, S., 2020. Flavonoids as alpha-glucosidase inhibitors: Mechanistic approaches merged with enzyme kinetics and molecular modelling. Phytochem. Rev. 19, 1081–1092. https://doi.org/10.1007/s11101-019-09610-6.

Şöhretoğlu, D., Sari, S., Barut, B., et al., 2018. Discovery of potent α-glucosidase inhibitor flavonols: Insights into mechanism of action through inhibition kinetics and docking simulations. Bioorg. Chem. 79, 257–264. https://doi.org/10.1016/j.bioorg.2018.05.010.

Sukhikh, S., Babich, O., Prosekov, A., et al., 2023. Antidiabetic properties of plant secondary metabolites. Metabolites 13, 513. https://doi.org/10.3390/metabo13040513.

Tran, N., Pham, B., Le, L., 2020. Bioactive compounds in anti-diabetic plants: From herbal medicine to modern drug discovery. Biology 9, 252. https://doi.org/10.3390/biology9090252.

World Health Organization, 1999. Definition, diagnosis and classification of diabetes mellitus and its complications: report of a WHO consultation. Part 1, Diagnosis and classification of diabetes mellitus.

Yuca, H., Özbek, H., Demirezer, L.Ö., et al., 2021. trans-Tiliroside: A potent α-glucosidase inhibitor from the leaves of Elaeagnus angustifolia L. Phytochemistry 188, 112795.

Zhou, R., Xiang, C., Cao, G., et al., 2021. Berberine accelerated wound healing by restoring TrxR1/JNK in diabetes. Clin. Sci. 135, 613–627. https://doi.org/10.1042/CS20201145.